aerospace

MDPI

Article

Experimental Study on Hypersonic Double-Wedge Induced Flow Based on Plasma Active Actuation Array

Bo Yang [1,2], Hesen Yang [3,*], Ning Zhao [1], Hua Liang [3,*], Zhi Su [3] and Dongsheng Zhang [3]

[1] College of Aerospace Engineering, Nanjing University of Aeronautics and Astronautics, Nanjing 210016, China; yandr_2002@139.com (B.Y.); zhaoam@nuaa.edu.cn (N.Z.)
[2] Hypervelocity Aerodynamics Institute of China Aerodynamics Research and Development Center, Mianyang 621000, China
[3] National Key Lab of Aerospace Power System and Plasma Technology, Air Force Engineering University, Xi'an 710038, China; suzhi95703@163.com (Z.S.); zds13475138164@163.com (D.Z.)
* Correspondence: yanghesen96@126.com (H.Y.); lianghua82702@163.com (H.L.)

Abstract: The double-wedge configuration is a typical characteristic shape of the rudder surface of high-speed aircraft. The impact of the shock wave/boundary layer interaction and the shock wave/shock wave interaction resulting from the double wedge on aircraft aerodynamics cannot be ignored. The aerodynamic performance of the aircraft would be seriously affected. Accordingly, to reduce the wave drag, and to relieve the thermal load and pressure load, flow control is required for the shock wave/shock wave interaction and the shock wave/boundary layer interaction induced by the double-wedge configuration. In this paper, double-wedge shock wave/shock wave interaction is controlled by a high-energy surface arc discharge array and observed by high-speed schlieren flow field measurement at Mach 8. The 30-channel discharge array is set on the primary wedge plane, and actuation is generated. Hypersonic V shock wave/shock wave interaction is effectively controlled by the shock wave array induced by the high-energy surface arc discharge array, which makes the shock wave/shock wave interaction structure disappear or intermittent. The potential control mechanism is to reduce strong shock wave interaction by transforming the type of shock wave interaction. Therefore, the ability of plasma array actuation to control complex shock wave/shock wave interaction is verified, which provides a new method for hypersonic shock wave/shock wave interaction control.

Keywords: hypersonic; surface arc discharge; plasma actuation; flow control; experimental research

Citation: Yang, B.; Yang, H.; Zhao, N.; Liang, H.; Su, Z.; Zhang, D. Experimental Study on Hypersonic Double-Wedge Induced Flow Based on Plasma Active Actuation Array. *Aerospace* **2024**, *11*, 60. https://doi.org/10.3390/aerospace11010060

Academic Editor: Zhijin Wang

Received: 28 October 2023
Revised: 28 December 2023
Accepted: 4 January 2024
Published: 9 January 2024

1. Introduction

Shock wave/shock wave interaction and shock wave/boundary layer interaction are widespread problems in high-speed flows, which are key problems restricting the development of a new generation of aircraft [1,2]. The double-wedge configuration is a prominent feature of high-speed aircraft, appearing in numerous areas, such as the control rudder surface, air body–wing joint, and multi-inclined compressed inlet [3–5]. Shock wave/boundary layer interaction and shock wave/shock wave interaction occurring within these hypersonic double-wedge flows induce a range of complex flow phenomena, including boundary layer separation and reattachment, unstable shear layer, supersonic jet, nonlinear shock wave oscillation, and hysteresis phenomenon. These phenomena are major obstacles that restrict the development of a new generation of aircraft [6]. The two kinds of interaction induce extreme thermal loads and pressure loads, and the complex flow environment further leads to load fluctuations, resulting in component damage or even loss of control of the aircraft in serious cases [7,8]. Consequently, in order to reduce wave drag and relieve thermal load and pressure load, it is necessary to carry out flow control for shock wave/shock wave interaction and shock wave/boundary layer interaction induced by the double-wedge configuration [9,10].

Complex shock wave/shock wave interaction and shock wave/boundary layer interaction under the condition of high-speed incoming flow bring about severe aerodynamic thermal loads and drastic changes in flow parameters, bringing serious challenges to the aircraft body structure and thermal protection [11,12]. The current passive protection measures cannot easily ensure the safety of aircraft, but if the load can disappear or temporarily rest by changing the wave system structure, it is expected to bring new ideas for the thermal protection design of high-speed aircraft [13,14]. Therefore, a control method that can effectively change the structure of a shock wave system without changing the surface characteristic shape of aircraft is needed.

Plasma flow control is a method to control fluid flow by using plasma technology, which belongs to active flow control means. It is mainly divided into dielectric barrier discharge, synthetic jet and surface arc discharge. Especially in the hypersonic field, surface arc discharge is widely used in solving shock wave/shock wave interaction and shock/boundary layer interaction, and lots of research has been carried out by scholars in the field.

In numerous current flow control experimental studies, Wang et al. experimentally verified the control ability of a surface arc plasma actuator to compress corner-inclined shock waves under Mach 6 flow [15]. Xie et al. used plasma synthetic jet actuation to achieve effective control of type VI shock wave/shock wave interaction on a double wedge. In the three working conditions, the longest control time was only 90 μs, the energy deposited into the flow field was above 4.1 J, and the repetition frequency was only 1 Hz [16]. However, surface arc plasma actuation shows excellent control effects in supersonic shock wave control, shock wave/boundary layer interaction, and forced supersonic boundary layer transition [17–20]. Yang conducted controlling hypersonic boundary layer transition using a surface arc plasma actuation array. The influence of three different actuation frequencies (8, 34, and 55 kHz) was studied based on linear stability theory analysis, and a transition criterion under the control of plasma actuation was proposed. Finally, the corresponding control mechanism was summarized, and the transition control mechanization was refined [17]. In addition, Yang experimented on the stability of the hypersonic plate boundary layer by using a spanwise plasma actuation array. The experimental results verify the ability of extensional array plasma actuation to control the stability of the hypersonic plate boundary layer, suggesting that it has great potential in the promotion of hypersonic boundary layer transition [18]. In addition, a wind tunnel experiment was carried out under the condition of Mach number 6 to study the stability adjustment of the hypersonic blade. The results verify the ability of plasma actuation to stimulate the instability of hypersonic cone boundary layers and provide technical support for the further development of transition control methods [19]. Kong et al. conducted experiments on the control of double-wedge flow by 10 discharge actuators under hypersonic conditions and analyzed the interaction evolution process between plasma surface arc discharge and a flow field in detail [21]. Ding et al. studied the unsteady control mechanism of pulsed surface arc discharge plasma on hypersonic compression corner flow by combining numerical simulations and experiments. The interaction mechanism between arc discharge plasma and hypersonic flow was revealed. The research reveals that the local Joule heat is created by the surface arc discharge, which also triggers the separation region near the wall, leading to an increase in local displacement thickness and the formation of an unsteady virtual wedge that moves along the wall. Consequently, an oblique shock wave is produced, with the shock angle varying with time, and an unsteady shock wave/shock wave interaction including shock reflection is established between the front wedge shock wave. The hot gas mass generated by the discharge demonstrates a significant capacity to control the oblique back wedge shock wave [22]. Although the conventional surface arc discharge electrode plays a certain role in controlling the hypersonic flow field, there is still a more urgent need for plasma discharge with more paths and larger affected areas, in order to obtain better control effects.

In order to further improve the ability of surface arc actuation to control complex shock wave/shock wave interaction and shock wave/boundary layer interaction induced by a double-wedge configuration in a wide velocity domain, a spanwise and flow-direction combination array actuator is designed in this paper to broaden the disturbance range and achieve effective control for typical shock wave interaction induced by a double-wedge configuration. The ability of array plasma actuation to control complex shock wave/shock wave interaction is verified.

2. Experimental System

The experiment is conducted in Φ0.5 m conventional hypersonic wind tunnel in the Hypervelocity Aerodynamics Institute of China Aerodynamics Research and Development Center. The whole experiment system mainly includes hypersonic wind tunnel, double-wedge model, plasma actuation system, high-speed schlieren system, synchronous control system, etc.

2.1. Hypersonic Wind Tunnel and Test System

The experiment was carried out in a hypersonic wind tunnel with a diameter of 0.5 m at the Hypervelocity Aerodynamics Institute of China Aerodynamics Research and Development Center. The wind tunnel is a conventional hypersonic wind tunnel with a simulated Mach number of 5–10 and a diameter of 0.5 mm (Mach number 5–8) and 0.6 mm (Mach number 9, 10), respectively. The total pressure range of the wind tunnel is 0.1–3 MPa, the total temperature range is 301–1073 K, and the unit Reynolds number is 1.5×10^5~6.0×10^7/m. The wind tunnel test section is shown in Figure 1. There are relatively few studies on the double-wedge flow control under hypersonic conditions. The maximum Mach number of wind tunnel operation is Mach 8, and studies on the double-wedge problem under higher Mach number are more valuable; there are fewer studies on the double-wedge problem under Mach 8 conditions. Therefore, Mach 8 is chosen as the experimental condition, and the experimental model is designed under this condition. In addition, for other flow conditions, considering the high-altitude aircraft environment and plasma discharge environment, a total pressure of 3 MPa and a total temperature of 410 K are selected. After determining the total pressure, total temperature, and Mach number, other test conditions can be determined. The experimental flow parameters are shown in Table 1.

Figure 1. Hypersonic wind tunnel and test section.

Table 1. Main parameters of incoming stream.

Ma_∞ (U_∞/c)	Re/m ($\rho U_\infty/\mu$)	U_∞ (m/s)	ρ (kg/m^3)	P_0 (MPa)	T_0 (K)	P_S (Pa)	T_S (K)
8.0	6.16×10^6	874.292	0.036	3	410	307.287	29.710

Ma_∞, Re/m, U_∞, ρ, P_0, T_0, P_S, T_S, c represent incoming Mach number, unit Reynolds number, free flow velocity, incoming density, total pressure, total temperature, static pressure, static temperature, and sound velocity.

2.2. Double-Wedge Model and Actuator

The model consists of a first-stage wedge, a second-stage wedge, a support, and a plasma actuator. Among them, because the primary wedge is at the front of the model, it will be subjected to strong aerodynamic heating in the hypersonic flow field, so alumina ceramic material is used to prevent its tip from deformation or damage at high temperature. In the flow field, double wedge will generate separation shock waves, and there are shock waves on its surface. However, compared with the tip of the first-stage wedge, the surface of the second-stage wedge is not easily deformed. The second-stage wedge is made of PEEK (poly-ether-ether-ketone) material. The actuator is embedded in the support, and in order to prevent the ablation caused by discharge, the whole alumina ceramic is processed. The model support is made of plexiglass material.

The size of the model is shown in Figure 2. The streamwise direction length is 240 mm, the normal height is 177 mm, and the angle of the first-stage wedge is 30°; the angle of the second-stage wedge is 60°. The actuator array is located 15 mm upstream of the second-stage wedge, the electrode gap is 0.5 mm, and the flow distance between the two adjacent actuators is 9 mm. The arrangement of two columns × 15 channels of flow direction is adopted, and there are 30 channels of actuators in total. For the driver design, in addition to the needle electrode at both ends, the middle electrode is U-shaped, and the ceramic cover plate is used for packaging.

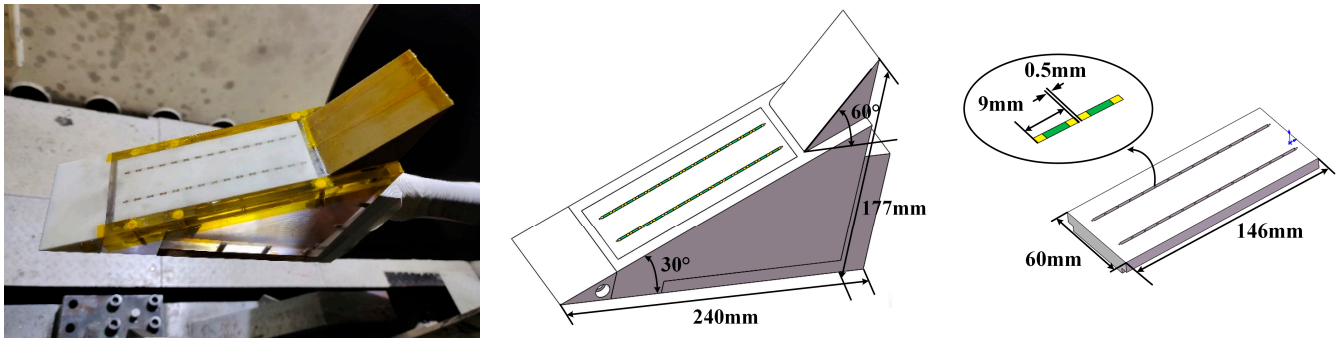

(**a**) (**b**) (**c**)

Figure 2. Double wedge model. (**a**) Installation of the model in the wind tunnel; (**b**) model parameter. (**c**) The details of the actuator.

2.3. The Power Supply System and Schlieren System

The power supply system consists of a nanosecond pulse power supply and a low-power DC power supply. The input voltage of both power supplies is 220 V and the input frequency is 50 Hz. The nanosecond pulse power supply is manufactured by China Xi'an Lingfeng Yuan Electronic Technology Co. The peak voltage range of the nanosecond pulse power supply is 0–20 kV, and the discharge pulse frequency is 0–20 kHz. The low-power DC power supply is manufactured by Jiangsu, China of Zhengjie power factory. DC power output ranges from 0 to 1.2 kV. The electrical parameter-measuring equipment is composed of an oscilloscope, voltage probe, and current ring. The discharge loop is connected to a micronormal capacitor, a diode, and a current-limiting resistor. Two power sources are connected in the circuit, in which the nanosecond pulse power supply can

provide instantaneous pulse high voltage, quickly break down the discharge gap between the positive and negative electrodes of the driver, and establish a discharge channel. The DC power supply charges the capacitor through the resistance, storing the energy in the capacitor. When the discharge gap is broken down, the capacitor quickly releases the energy through the discharge channel, producing a high-energy plasma actuation. Under the operation of this circuit, the peak output current can reach an order of 100 A, and the deposited energy can reach the order of 1 J.

Instantaneous snapshot by high-speed schlieren is the most commonly used test method in high-speed flow experiments. It does not interfere with the flow field, maintains the authenticity and accuracy of the original flow field, and can capture the change in density gradient in the flow field, thus revealing the detailed structure in the flow field. In order to observe the flow field structure and wave system of shock wave interaction, a high-speed schlieren system is used in this experiment. The schlieren light path is set in a Z-shape light path. The structure of the flow field is captured by a high-speed schlieren system. The schlieren light path is set in a Z-shape light path. The high-speed camera uses a Phantom V2512 high-speed CCD camera (Phantom, Vision Research, Wayne, NJ, USA) to record images at a sampling frequency of 75,000 fps and an exposure time of 9 μs. For the optical setting, through the early debugging, the coupling effect of exposure time, aperture, and light source intensity is the best, which better reflects the experimental results.

2.4. Research Methods

A grayscale image is a two-dimensional data structure that represents an image through the intensity value of each pixel in the range of grayscale values, generally used to depict information on black-and-white or grayscale intensity but not color. In this experiment, we utilize the mean gray-level processing method to process the spatial gray-level image. This entails calculating the average intensity value of each pixel in the image time series. Based on the time-resolved schlieren space gray image, this paper also analyzes the decomposition through root mean square (RMS) and Snapshot proper orthogonal decomposition (SPOD). Although schlieren display technology is mainly used for qualitative flow field diagnosis, some post-processing methods based on schlieren snapshot sequences have also been developed rapidly in recent years, which are used to extract semi-quantitative data from a large number of qualitative schlieren data and then initially reveal some quantitative flow field results [23]. In this paper, in addition to analyzing the instantaneous schlieren results, statistical processing is performed on the obtained schlieren image sequence to obtain its average schlieren intensity field (I_{mean}) and RMS schlieren intensity field (I_{rms}), which are specifically defined as follows:

$$I_{mean} = \sum_{k=1}^{N} I_k / N \tag{1}$$

$$I_{rms} = \sqrt{\sum_{k=1}^{N} (I_k - I_{mean})^2 / N} \tag{2}$$

where I_k is the gray value matrix of pixels in the kth schlieren snapshot; N is the total sample number of the schlieren snapshot sequence.

The average gray value is the schlieren diagram of the steady flow field. The flow pulsation state can be obtained by calculating the root mean square of the time series of the gray level of spatial pixels.

Proper orthogonal decomposition (POD), as a principal component analysis method, decomposes the flow field into different modes according to the contribution rate of the flow field, which can filter out the secondary structure and noise in the flow field and obtain the main flow structure. POD method is widely used in experimental and simulation data to study turbulence characteristics. Data obtained by PIV technology and LES simulation method can be processed by POD method to obtain spatial flow topology of velocity and

vortex structure [24]. Berry et al. [25] used POD method to process time series of time-resolved schlieren images and studied the characteristic structure of supersonic rectangular jet. Chaganti et al. [26] processed a time series of color schlieren images and studied the non-steadiness of shock wave/boundary layer interaction.

However, fast orthonormal decomposition (SPOD) mainly analyzes the correlation in multiple pictures distributed along the time axis for points in the same position [27]. The modes obtained by SPOD decomposition have the following characteristics: the lower the mode order, the higher the contribution rate to the flow field; the modes with high contribution rate represent the dominant structure of the flow field. The first mode has the highest contribution rate and usually reflects the steady-state information of the flow field. Steady-state characteristics have been studied in gray mean or root-mean-square analysis. The advantage of SPOD analysis method is to extract unsteady characteristics of flow field [26].

In the process of experiment, in order to ensure that statistical results are obtained under the same number of samples, 300 instantaneous schlieren snapshots after actuation are uniformly selected as statistical sample values (300 instantaneous schlieren snapshots are also selected for the base flow field).

3. Study on Base Interaction Flow Field

In order to clarify the structure of the shock wave in the flow field and determine the type of shock wave/shock wave interaction, the schlieren image is analyzed. As shown in Figure 3, the instantaneous schlieren snapshot of the base flow field at Mach 8.0 is given, where the flow direction and normal coordinate scales are dimensionless, processed by the model length and height, respectively. According to the schlieren display results, the base flow field of the double-wedge model is the normal intersection of the same side shock wave at the two Mach numbers. The oblique shock wave AC generated by the first-stage wedge and the oblique shock wave BC generated by the second-stage wedge intersect at point C, and the transmitted shock wave CD is generated. The shock angle of CD is smaller than BC but larger than AC. Subsequently, in order to balance the pressure between regions ④ and ③ behind shock wave CD and shock wave BC, the wave structure CF is induced. Notice that CE here is not a simple slip line but a supersonic jet. At the same time, it can be clearly observed that there are two multi-wave points, C and C′, in the interfering flow field. The results show that Edney's typification of the shock/shock interaction phenomenon is also applicable to hypersonic ranges. Therefore, according to a comprehensive judgment, the benchmark interfering flow field shown in Figure 3 is the type V shock wave/shock wave interaction.

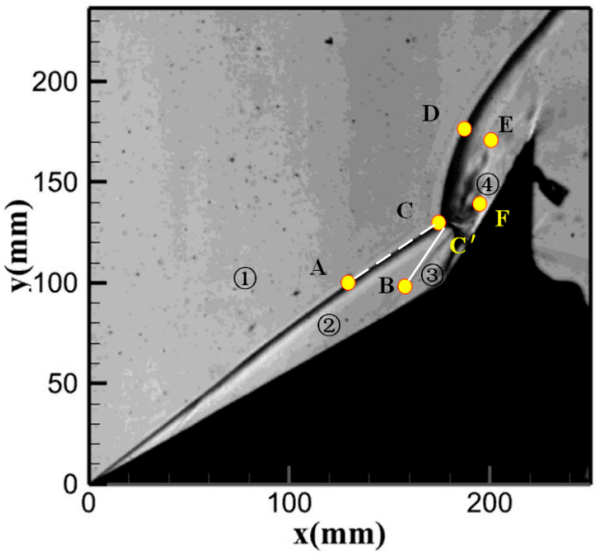

Figure 3. Base flow field of double-wedge model at Mach 8.

4. The Control Effect of Array Plasma Actuation

The interaction flow field induced by a double wedge under the actuation of 30-channel discharge is shown in Figure 4. Since the discharge arrangement of the actuator is two rows and 15 channels, 15 shock wave and hot gas cluster arrays can be clearly seen from the figure, indicating that the discharge is successful at Ma 8. It can also be seen from the figure that with the generation of plasma actuation, the flow field structure changes, the shape of the first-stage wedge precursor of the experimental model bends and deforms, and the type V shock wave/shock wave interaction on the surface of the second-stage wedge is significantly weakened, which indicates that the arc plasma actuation achieves effective control of the flow field wave system.

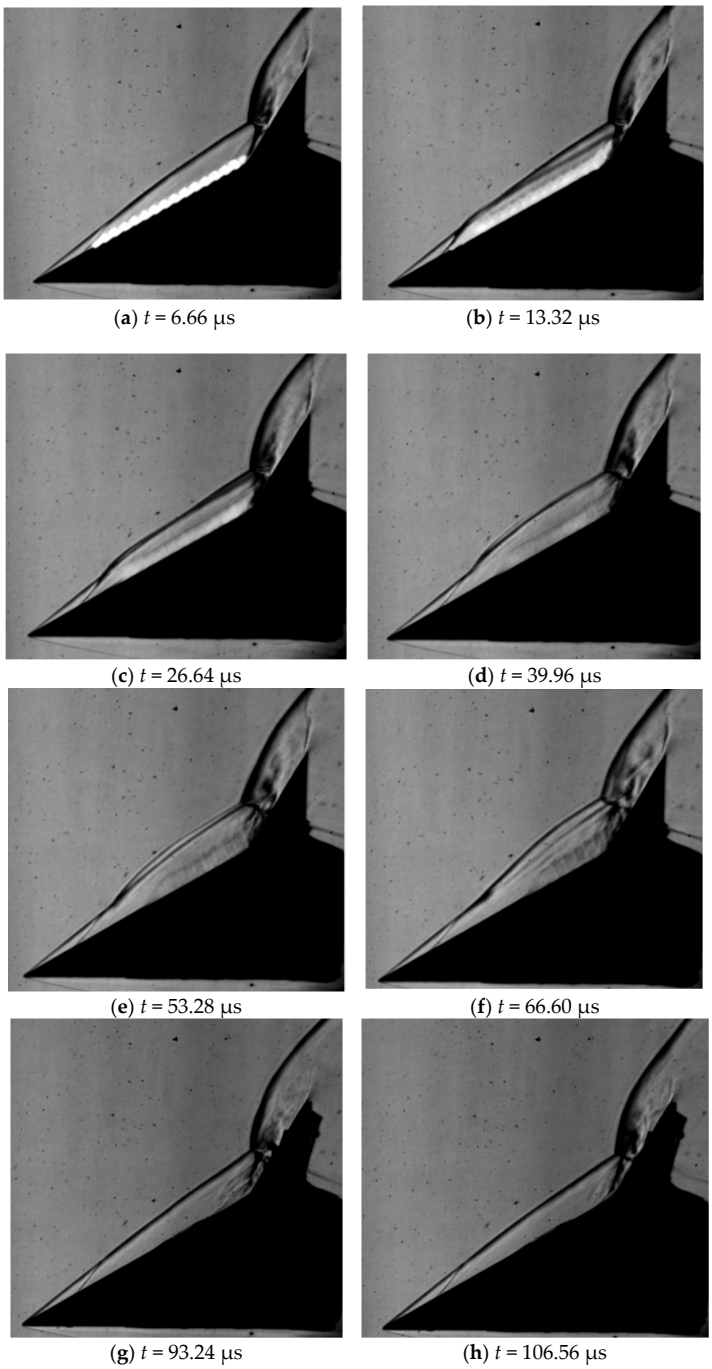

(**a**) t = 6.66 μs (**b**) t = 13.32 μs

(**c**) t = 26.64 μs (**d**) t = 39.96 μs

(**e**) t = 53.28 μs (**f**) t = 66.60 μs

(**g**) t = 93.24 μs (**h**) t = 106.56 μs

Figure 4. Thirty-channel discharge control of shock wave/boundary layer interaction induced by double wedge.

Through detailed comparative analysis, the control evolution process of a discharge pulse on a double-wedge flow field can be divided into two stages, namely, the disappearance of the shock wave interaction structure and the reconstruction of the shock wave interaction structure.

As shown in Figure 4b, at the initial discharge moment (t = 0 μs), 30 arc arrays with spanwise overlap are observed on the surface of the model. After 6.66 μs, the arc array develops into a dazzling white light due to energy deposition in a short time. Subsequently, as shown in Figure 4d, the actuation induced by the plasma bulge makes the impact shock wave AC appear arched, while the second-stage pre-wedge oblique shock wave BC disappears. In the next two moments, with the expansion of the plasma bulge, the shock wave and interaction structure in front of the wedge disappear, leaving only a bow shock wave. As shown in Figure 4f, the plasma bulge changes into a plasma wedge, and the bow shock wave in the flow field also changes into an oblique shock wave.

At the time of t = 53.28 μs, as shown in Figure 4e, the second-stage pre-wedge oblique shock wave BC begins to reconstruct. Then, as shown in Figure 4f, the oblique shock wave BC appears completely but its shape is distorted, and the interaction structure does not appear. At the time of t = 93.24 μs, the transmitted shock wave appears, and the interaction structure begins to rebuild. The flow field returns to the state before actuation until t = 106.56 μs; then, the control of array plasma actuation flow field ends.

According to the analysis of static discharge results, at Mach 8, the shock wave array successively forms a plasma bulge and plasma wedge, resulting in shock wave deformation, while the hot gas mass directly causes the disappearance of the shock wave interaction structure in the process of downstream expansion, and the array plasma actuation shows the control ability of double-wedge flow.

4.1. Results of Gray Average and RMS

Firstly, the overall control effect of thirty surface arc actuations on hypersonic interaction flow field induced by a double-wedge is measured by gray average results and RMS results, as shown in Figures 5 and 6.

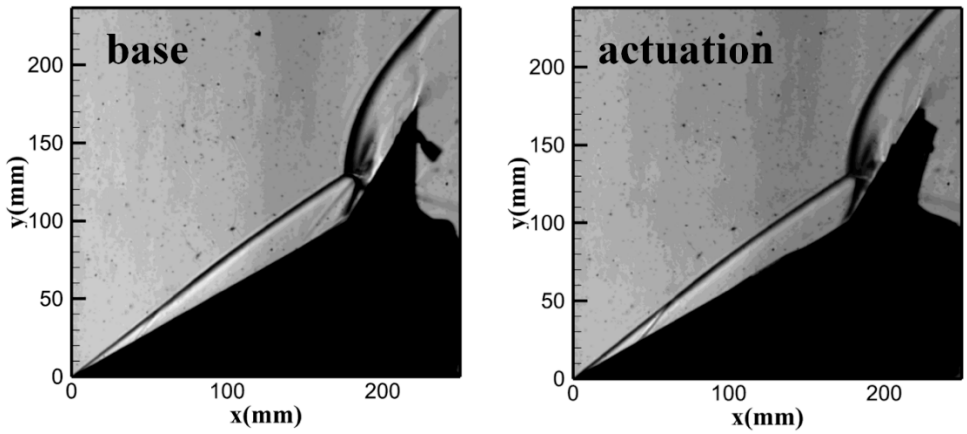

Figure 5. The control effect of gray average.

In the gray average results, it is obvious that the intensity of the oblique shock wave BC generated by the second-stage wedge decreases obviously under the shock wave induced by the array actuation, while the interaction point of the type V shock wave induced by the double wedge does not change significantly. In the control effect of RMS, the pulsation region of the shock wave induced by actuation can be observed. Most importantly, the pulsation level of a type V shock wave induced by the double wedge is enhanced near the shock disturbance point. Therefore, the introduction of array plasma actuation has a positive control effect on the shock disturbance point.

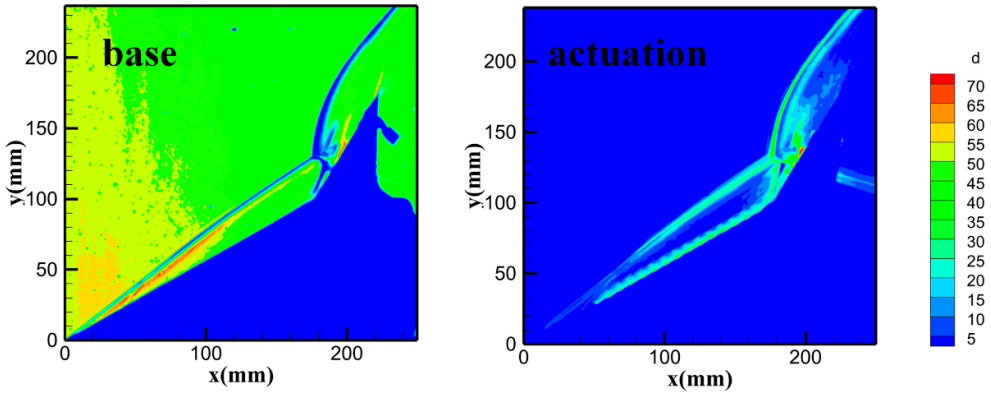

Figure 6. The control effect of RMS.

4.2. Results of SPOD Analysis

SPOD decomposes the flow field into a series of modes to extract the coherent structure in the flow field. The time series of 300 images of the base flow field is decomposed by SPOD, and each mode is sorted according to the energy contribution rate from the largest to the smallest. The lower the mode order, the greater the energy contribution rate to the original flow field. Thus, 300, 500, and 1000 photos are selected for processing, and the results are found to be basically the same, so the processing results of 300 photos are displayed.

As shown in Figure 7, the energy proportion of each unsteady mode analyzed by SPOD is shown. It can be seen that the energy proportion of the first several unsteady modes is very high, and the unsteady mode energy accumulation value of the first ten modes reaches more than 99.94%. Therefore, the first ten modes are selected to analyze the modal results of the base interaction flow field and the actuation control flow field. The results are shown in Figure 8.

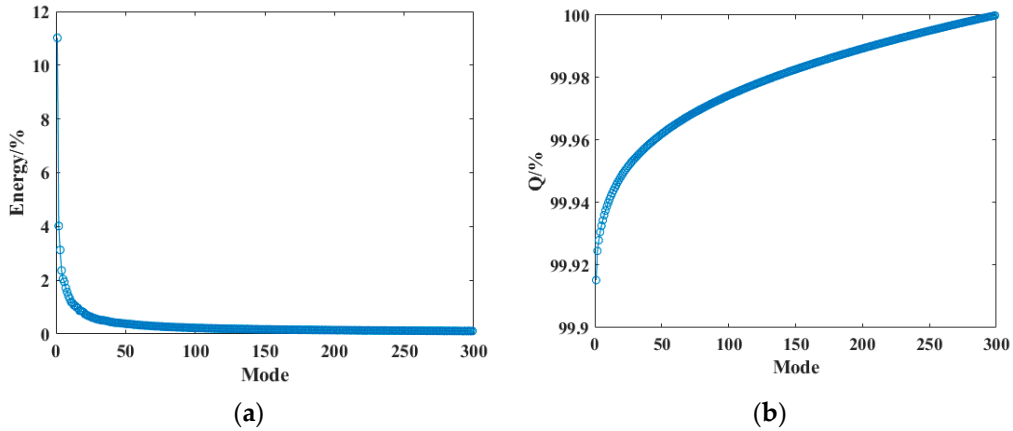

Figure 7. The energy proportion of each mode analyzed by SPOD. (**a**) Unsteady modal energy distribution; (**b**) unsteady mode energy accumulation value.

From the SPOD results, it can be seen that in the benchmark SPOD results, the obvious second wedge oblique shock wave and shock disturbance point are observed both in the steady-state mode (mode 1) and other unsteady modes. Since MOD1 is a steady-state mode, it can be found that the color of the red region in the actuation flow field is lighter than that of the base flow field, indicating that the shock wave intensity is weakened under the condition of plasma actuation, and the plasma arc discharge plays a role in regulating the shock wave. In the unsteady mode results, mode 2, mode 3, mode 4, and mode 5 are the actuation modes. The first shock wave structure or the second shock wave structure can be obviously observed in both the base flow field and the actuation flow field, and

the energy of the shock wave structure is still dominant. In addition, the shock wave driven by the array plasma can also be clearly observed from MOD2–5. It shows that the energy stimulated by the MOD2–5 plasma also occupies a certain dominant position in the actuation flow field. The latter unsteady mode is the shock wave/shock wave interaction control mode, and it can be observed that the display degree, which decreases after the shock wave interaction point, is affected. Therefore, on the basis of the SPOD analysis results, the display of the double-wedge oblique shock wave controlled by plasma is reduced after processing, the control effect of the array plasma actuation on the shock wave/shock wave interaction is verified, and the intensity of the double-wedge oblique shock wave is weakened.

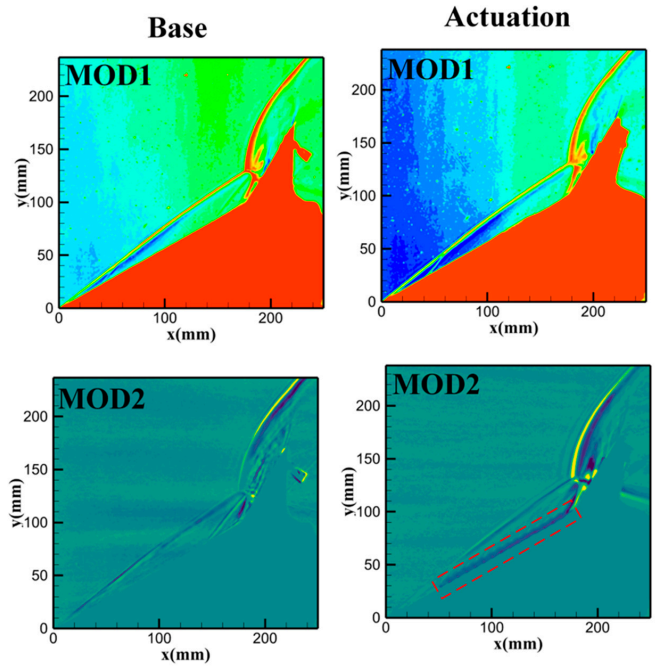

(**a**)

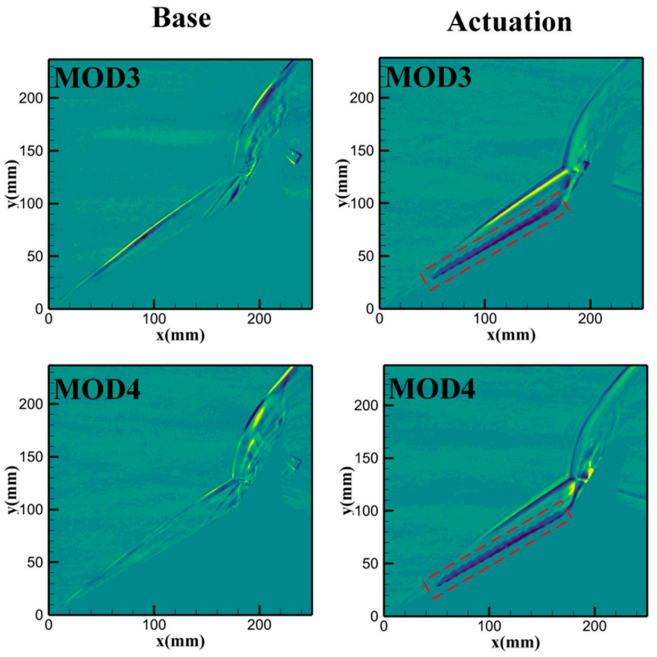

(**b**)

Figure 8. *Cont.*

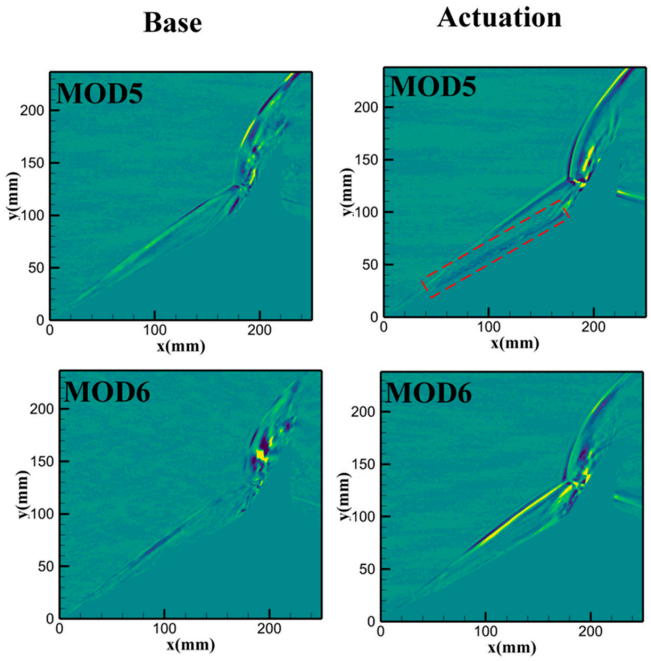

(**c**)

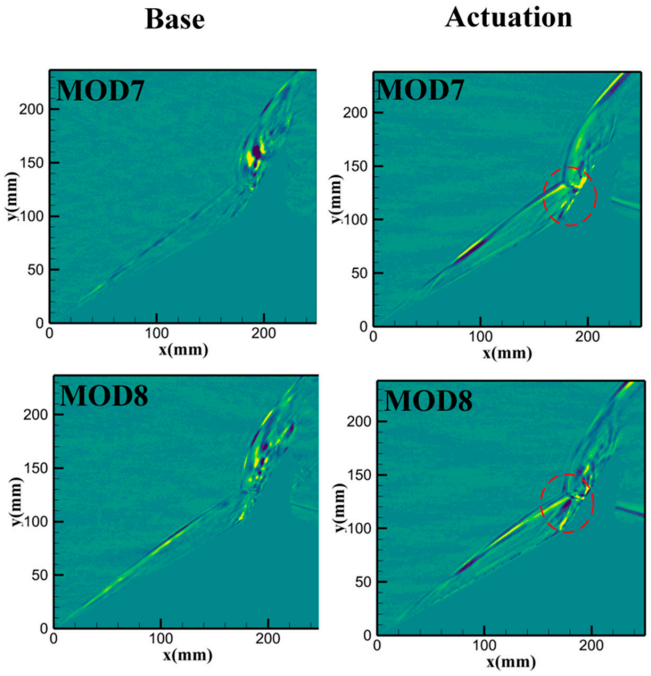

(**d**)

Figure 8. *Cont*.

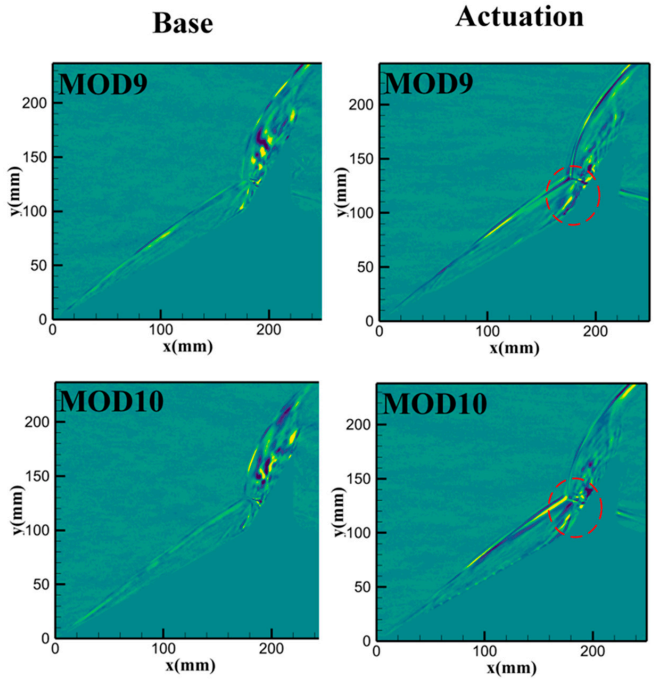

(**e**)

Figure 8. The results of each mode analyzed by SPOD. (**a**) MOD1, 2; (**b**) MOD3, 4; (**c**) MOD5, 6; (**d**) MOD7, 8; (**e**) MOD9, 10.

Another control effect that needs attention is the ④ region defined in Figure 3, where each SPOD mode shows that the supersonic jet emitted by point C has been effectively controlled and has a tendency to develop into a complete slip line. Therefore, it can be inferred that, by the control of the shock wave/shock wave interaction structure, the final control mechanism formed by the array surface arc actuation may be to convert the type V shock wave/shock wave interaction type, with more intense interaction and more complex flow field into the type VI shock wave/shock wave interaction type during the change in the shock mechanism.

5. Conclusions

In this paper, a high-speed schlieren flow field test method is used to study the Ma8 hypersonic double-wedge shock wave interaction controlled by a high-energy surface arc discharge array. As a new type of super multipath discharge, 30 channels are used in the double-wedge mode. A 30-channel discharge array is set on the first-stage wedge surface, and actuation is applied to the interaction flow field. The shock wave array and the hot gas array induced by the high-energy surface arc discharge array develop into a virtual bulge and wedge in the hypersonic double wedge. Under the action of the virtual wedge, the complex double-wedge shock disturbance structure evolves into a bow shock wave or an oblique shock wave. The results show that the ultra-multi-array surface arc actuation used in this paper can effectively control hypersonic Type V shock wave/shock wave interaction, making the shock wave/shock wave interaction structure disappear or be intermittent, and the new surface arc discharge plays a better role in regulating the shock wave. The potential control mechanism is to mitigate the strong interaction caused by shock wave/shock wave interaction by transforming the type of shock wave/shock wave interaction. This verifies the ability of array plasma actuation to control complex shock wave/shock wave interaction and provides a new type of plasma surface arc discharge and a new method for hypersonic shock wave/shock wave interaction control.

Author Contributions: Conceptualization, B.Y. and H.Y.; methodology, B.Y. and H.Y.; software, H.Y.; validation, H.L., H.Y. and D.Z.; formal analysis, B.Y.; investigation, H.Y.; resources, N.Z.; data curation,

D.Z.; writing—original draft preparation, B.Y.; writing—review and editing, H.Y.; visualization, Z.S.; supervision, H.L.; project administration, H.L.; funding acquisition, H.L. All authors have read and agreed to the published version of the manuscript.

Funding: This research was funded by the National Science and Technology Major Project (Grant No. J2019-II-0014-0035).

Data Availability Statement: The data and materials are available upon request.

Acknowledgments: Thanks to Cao Jingqi and Wang Shaoyi for their help in the experiment.

Conflicts of Interest: The authors declare no conflicts of interest.

References

1. Boyd, I.D.; Chen, G.; Candler, G.V. Predicting failure of the continuum fluid equations in transitional hypersonic flows. *Phys. Fluids* **1995**, *7*, 210–219. [CrossRef]
2. Lee, C.; Chen, S. Recent progress in the study of transition in the hypersonic boundary layer. *Natl. Sci. Rev.* **2019**, *6*, 155–170. [CrossRef] [PubMed]
3. Castrogiovanni, A. Review of "The Scramjet Engine, Processes and Characteristics". *AIAA J.* **2010**, *48*, 2173–2174. [CrossRef]
4. Devaraj, M.K.K.; Jutur, P.; Rao, S.M.V.; Jagadeesh, G.; Anavardham, G.T.K. Experimental investigation of unstart dynamics driven by subsonic spillage in a hypersonic scramjet intake at Mach 6. *Phys. Fluids* **2020**, *32*, 026103. [CrossRef]
5. Kimmel, R.L. Aspects of hypersonic boundary layer transition control. In Proceedings of the 41st Aerospace Sciences Meeting and Exhibit, Reno, NV, USA, 6–9 January 2003.
6. Raj, N.O.P.; Venkatasubbaiah, K. A new approach for the design of hypersonic scramjet inlets. *Phys. Fluids* **2012**, *24*, 086103. [CrossRef]
7. Borg, M.P.; Schneider, S.P. Effect of Freestream Noise on Roughness-Induced Transition for the X-51A Forebody. *J. Spacecr. Rockets* **2008**, *45*, 1106–1116. [CrossRef]
8. Everhart, J.L.; Alter, S.J.; Merski, N.R. Pressure gradient effects on hypersonic cavity flow heating. In Proceedings of the 44th AlAA Aerospace Sciences Meeting and Exhibit, Reno, NV, USA, 6–9 January 2006.
9. Brès, G.A.; Inkman, M.; Colonius, T.; Fedorov, A.V. Second-mode attenuation and cancellation by porous coatings in a high-speed boundary layer. *J. Fluid. Mech.* **2013**, *726*, 312–337. [CrossRef]
10. Fujii, K. Experiment of the Two-Dimensional Roughness Effect on Hypersonic Boundary-Layer Transition. *J. Spacecr. Rocket.* **2006**, *43*, 731–738. [CrossRef]
11. Zhang, S.; Li, X.; Zuo, J.; Qin, J.; Cheng, K.; Feng, Y.; Bao, W. Research progress on active thermal protection for hypersonic vehicles. *Prog. Aerosp. Sci.* **2020**, *119*, 100646. [CrossRef]
12. Zhu, Y.; Peng, W.; Xu, R.; Jiang, P. Review on active thermal protection and its heat transfer for airbreathing hypersonic vehicles. *Chin. J. Aeronaut.* **2018**, *31*, 1929–1953. [CrossRef]
13. Le, V.T.; Ha, N.S.; Goo, N.S. Advanced sandwich structures for thermal protection systems in hypersonic vehicles: A review. *Compos. B Eng.* **2021**, *226*, 109301. [CrossRef]
14. Terentieva, V.S.; Astapov, A.N. Conceptual Protection Model for Especially Heat-Proof Materials in Hypersonic Oxidizing Gas Flows. *Russ. J. Non-Ferr. Met.* **2019**, *59*, 709–718. [CrossRef]
15. Wang, H.; Hu, W.; Xie, F.; Li, J.; Jia, Y.; Yang, Y. Control effects of a high-frequency pulsed discharge on a hypersonic separated flow. *Phys. Fluids* **2022**, *34*, 066102. [CrossRef]
16. Xie, W.; Luo, Z.; Zhou, Y.; Gao, T.; Wu, Y.; Wang, Q. Experimental study on shock wave control in high-enthalpy hypersonic flow by using SparkJet actuator. *Acta Astronaut.* **2021**, *188*, 416–425. [CrossRef]
17. Yang, H.; Liang, H.; Zhang, C. Plate boundary layer transition regulation based on plasma actuation array at Mach 6. *Phys. Fluids* **2023**, *35*, 064104.
18. Yang, H.; Liang, H.; Zhang, C.; Wu, Y.; Li, Z.; Zong, H.; Su, Z.; Yang, B.; Kong, Y.; Zhang, D.; et al. An experimental study on the stability of hypersonic plate boundary layer regulated by a plasma actuation array. *Phys. Fluids* **2023**, *35*, 026112. [CrossRef]
19. Yang, H.; Liang, H.; Zhang, C.; Wu, Y.; Zong, H.; Su, Z.; Kong, Y.; Zhang, D.; Li, Y. Investigation of hypersonic cone boundary layer stability regulation with plasma actuation. *Phys. Fluids* **2023**, *35*, 024112. [CrossRef]
20. Yang, H.; Zong, H.; Liang, H.; Wu, Y.; Zhang, C.; Kong, Y.; Li, Y. Swept shock wave/boundary layer interaction control based on surface arc plasma. *Phys. Fluids* **2022**, *34*, 087119. [CrossRef]
21. Kong, Y.; Li, J.; Wu, Y.; Liang, H.; Guo, S.; Yang, H. Experimental study on shock-shock interaction over double wedge controlled by surface arc plasma array. Contrib. *Plasma Phys.* **2022**, *62*, e202200062.
22. Ding, B.; Chen, Z.; Jiao, Z.; Wang, J.; Li, Z.; Bai, G. Unsteady control mechanisms of hypersonic compression corner using pulsed surface arc discharg. *Acta Aeronaut. Astronaut. Sin.* **2023**, *44*, 127744. (In Chinese)
23. Zhang, C.; Yang, H.; Liang, H.; Guo, S. Plasma-based experimental investigation of double compression ramp shock wave/boundary layer interaction control. *J. Phys. D Appl. Phys.* **2022**, *55*, 325202. [CrossRef]
24. Von Terzi, D.; Sandberg, R.; Sandberg, R.; Fasel, H. Identification of large coherent structures in supersonic axisymmetric wakes. *Comput. Fluids* **2009**, *38*, 1638–1650. [CrossRef]

25. Berry, M.; Magstadt, A.; Glauser, M. Application of POD on time-resolved schlieren in supersonic multi-stream rectangular jets. *Phys. Fluids* **2017**, *29*, 020706. [CrossRef]
26. Chaganti, N.; Kurup, A.; Olcmen, S. Study of unsteadiness of shock wave boundary layer interaction using Rainbow Schlieren Deflectometry and Proper Orthogonal Decomposition. In Proceedings of the AIAA Aerospace Sciences Meeting Including the New Horizons Forum & Aerospace Exposition, Grapevine, TX, USA, 7–10 January 2013.
27. Wang, H.; Min, F.; Xie, Z.; Li, J.; Dai, J.; Yang, Y. Quantitative study of the control of hypersonic aerodynamics using millisecond pulsed discharges. *Phys. Fluids* **2022**, *34*, 021701. [CrossRef]